Dynamic molecular collision (DMC) model for rarefied gas flow simulations by the DSMC method

T. Tokumasu and Y. Matsumoto
Department of Mechanical Engineering, The University of Tokyo, Hongo, Bunkyo-ku, Tokyo 113-8656, Japan

(Received 17 August 1998; accepted 7 April 1999)

The Dynamic Molecular Collision (DMC) model is constructed for accurate and realistic simulations of rarefied gas flows of nonpolar diatomic molecules by the Direct Simulation Monte Carlo (DSMC) method. This model is applicable for moderate temperatures (up to a few hundred K for nitrogen), where most molecules are in the vibrational ground state and the vibrational degree of freedom can be neglected. In this range, moreover, the rotational energy can be considered as a continuous one. The collisions of diatomic molecules are simulated many times by the Molecular Dynamics (MD) method at various initial conditions. The site to site potential is used as an intermolecular one. The collision cross section is developed from the database obtained by MD simulation and kinetic theory of viscosity coefficient of diatomic molecules. The probability density function of energy after collision is also developed using the database. In order to verify the DMC model, two flow fields are simulated. First, the DMC model is applied to the simulation of the translational and rotational energy distribution at the equilibrium condition and the results are compared with the Maxwell distribution. The results agree very well with each other. Second, the DMC model is applied to the simulation of the rotational relaxation through low and high Mach number normal shock wave. These results also agree very well with the experimental results of Robben and Talbot, although the upstream rotational temperature is a little lower. © *1999 American Institute of Physics.* [S1070-6631(99)02607-0]

I. INTRODUCTION

There is an increasing requirement to simulate highly nonequilibrium rarefied gas flows such as the shock wave generated at the space plane when it reenters the atmosphere, or the free-expansion jet to make a molecular beam for thin films produced in semiconductor fabrication. Relaxation of diatomic molecules in nonequilibrium flows is very different from that of monatomic molecules due to the internal degrees of freedom. It is important to study the effect of the internal degrees of freedom upon the energy transfer between colliding diatomic molecules.

The Direct Simulation Monte Carlo (DSMC) method is widely used to simulate rarefied gas flows. Many schemes to simulate the collision of molecules have been developed.[1–3] Previous studies have shown that the DSMC method is able to simulate monatomic rarefied gas flows very well.[1] Polyatomic rarefied gas flows, however, in which the gas molecules are able to transfer energy among translational, rotational and vibrational degrees of freedom cannot be accurately predicted using simple collision models. Larsen and Borgnakke[4] modeled the energy transfer between translational and internal degrees of freedom by assuming that the total energy is redistributed statistically using the appropriate equilibrium distribution function with an unrealistic constant rotational collision number Z_R to restrict the energy transfer. Parker[5] developed the variable rotational collision number, Z_R, using classical mechanics and Boyd[6–9] improved the Larsen Borgnakke (LB) model by using Parker's expression for variable Z_R. The profiles of the number density and rotational temperature of a shock wave agree well with experimental results by Robben and Talbot[10] with some adjustable parameters. Koura proposed the Statistical Inelastic Cross Section (SICS) model,[11,12] which assumes local detailed balance and employs Parker's rotational energy gain function. These results have slightly better agreement with the experimental data of Robben and Talbot compared to other models. It can be said, however, that all of these models are unable to predict the nonequilibrium condition, because they assume some unrealistic conditions like local equilibrium, which cannot be assumed in a strong nonequilibrium condition, and the adjustable parameters must be determined so that the results are consistent with the experimental results. The Classical Trajectory Calculations (CTC) DSMC method[13] is based on the collision dynamics, and it can be applied to the strong nonequilibrium condition like a high Mach number shock wave. The results agree with experimental results without any adjustable parameters. This method, however, is not practical to simulate a large flow field because the state of molecules after collision must be calculated by the Molecular Dynamics (MD) method directly and this requires a very large computation time.

In the present study, the Dynamic Molecular Collision (DMC) model for nonpolar diatomic molecules is constructed based on the collision dynamics like the CTC-DSMC method. This model can be applied to predict strong

nonequilibrium flows without adjustable parameters because the unrealistic condition like local equilibrium is not assumed in this model. In our method, however, the state of molecules after collision is determined by the model function derived by the MD simulation instead of the direct MD simulation in case of the CTC-DSMC method. Therefore, the simulation time of our method becomes much smaller than the CTC-DSMC method. To make the data referred to in the DSMC simulation, a large number of inelastic collisions of diatomic molecules are simulated by using the MD method for nitrogen. The detailed method of this simulation is written in Sec. II. The Lennard-Jones (LJ) potential between atoms is obtained based on the results of van der Avoird, Wormer and Jansen.[14–16] The detailed properties of the state of molecules after collision are discussed. The validity of the LJ potential is also discussed in this section. The DMC model is developed in Sec. III. The kinetic equation of the viscosity coefficient of diatomic molecules is used to determine the total collision cross section. The integral part of this equation is estimated by the database obtained by the MD simulation. For shorter simulation time, the inelastic cross section is defined based on the amount of energy transfer. The model probability density function of translational and rotational energy after collision is defined to reproduce the statistical property of that obtained by the MD simulations. They are constructed so that the initial energy of the collision molecules is the only independent variable. A database for the collision cross section and the probability density function is constructed for the DMC model. To make sure of its validity, this model is applied to two DSMC simulations in Sec. IV. The null-collision[17] technique is used to estimate the collision number in each cell. First, the translational and rotational energy distributions at the equilibrium condition are simulated and the results are compared with the Maxwell distribution. Second, the rotational relaxation of nitrogen in the low and high Mach number normal shock wave is simulated. The profiles of number density, rotational temperature and the relaxation of rotational energy distributions are compared with the experimental results of Robben and Talbot.[10]

II. MOLECULAR DYNAMICS SIMULATION

A large number of collision of diatomic molecules must be simulated by the MD method. Nitrogen, N_2, molecules are used as the collision molecules. Since the DMC model is constructed to simulate the flow field at moderate temperatures (about several hundred K), both collision molecules can be assumed as rigid rotators, and vibration and dissociation of the molecules can be neglected. Moreover, the quantum effect of rotational energy can be ignored and the rotational energy can be assumed as a continuous one.

A. Intermolecular potential

In the present study, the intermolecular potential is described as the sum of the four interatomic potentials. The interatomic potential is taken to be the Lennard-Jones (12-6) potential of the form

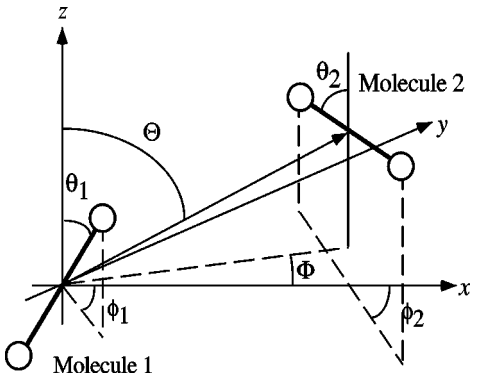

FIG. 1. The coordinate system used to calculate the averaged interatomic potential parameters.

$$V(r_{ij}) = 4\varepsilon_a \left\{ \left(\frac{\sigma_a}{r_{ij}} \right)^{12} - \left(\frac{\sigma_a}{r_{ij}} \right)^{6} \right\}, \tag{1}$$

where r_{ij} is the distance between atom i of molecule 1 and atom j of molecule 2. The potential parameters, $(\sigma_a, \varepsilon_a)$, are determined by comparison with the intermolecular potential obtained by *ab initio* calculation, hereafter called ''van der Avoird, Wormer and Jansen (AWJ) potential.''[14–16] As shown in Fig. 1, the system of the two rigid molecules is determined by the intermolecular relative position vector $\boldsymbol{R} = (R, \Theta, \Phi)$ of the center of mass of molecule 2 with respect to that of molecule 1 and the interatomic relative position vector $\boldsymbol{r}_i = (r_i, \theta_i, \phi_i)$ of the diatomic molecule $i(=1,2)$. In order to simplify the calculations, we have chosen a special frame with the z axis along $\boldsymbol{R}$ $(\Theta = \Phi = 0)$ and molecule 2 in the $x-z$ plane $(\phi_2 = 0)$. Since the interatomic distance r_i is invariant, only the internal coordinates $R, \theta_1, \phi_1, \theta_2$ are varied. The two potentials are expressed as $V(R, \theta_1, \theta_2, \phi_1)$.

The averaged AWJ potential at molecular distance R, $V^{\mathrm{ave}}_{\mathrm{AWJ}}(R)$, is calculated as

$$V^{\mathrm{ave}}_{\mathrm{AWJ}}(R) = \frac{1}{N_{\theta_1} N_{\theta_2} N_{\phi_1}} \sum_{i=1}^{N_{\theta_1}} \sum_{j=1}^{N_{\theta_2}} \sum_{k=1}^{N_{\phi_1}} V_{\mathrm{AWJ}}(R, \theta_{1i}, \theta_{2j}, \phi_{1k}), \tag{2}$$

by changing θ_{1i}, θ_{2j} and ϕ_{1k} as

$$\theta_{1i} = \cos^{-1} \frac{N_{\theta_1} - i}{N_{\theta_1}}, \quad \theta_{2j} = \cos^{-1} \frac{N_{\theta_2} - j}{N_{\theta_2}}, \quad \phi_{1k} = \frac{2\pi k}{N_{\phi_1}}, \tag{3}$$

where $N_{\theta_1} = 90$, $N_{\theta_2} = 90$, $N_{\phi_1} = 360$.

The averaged LJ potential $V^{\mathrm{ave}}_{\mathrm{LJ}}(R)$ at the potential parameters $(\sigma_a, \varepsilon_a)$ is calculated by the same method. The potential parameters $(\sigma_a, \varepsilon_a)$ are determined so that the difference between $V^{\mathrm{ave}}_{\mathrm{AWJ}}(R)$ and $V^{\mathrm{ave}}_{\mathrm{LJ}}(R)$ reaches a minimum. Thus the potential parameters, σ_a, ε_a, are determined as $\sigma_a = 3.17 \times 10^{-10}$ m and $\varepsilon_a = 6.52 \times 10^{-22}$ J.

The averaged AWJ and LJ potential curves are shown in Fig. 2. In this figure, the monatomic LJ potential obtained from the experimental data of viscosity coefficient[18] is also shown. The monatomic potential parameters, σ_m, ε_m are defined as $\sigma_m = 3.80 \times 10^{-10}$ m and $\varepsilon_m = 9.86 \times 10^{-22}$ J. As shown in this figure, the averaged AWJ potential and aver-

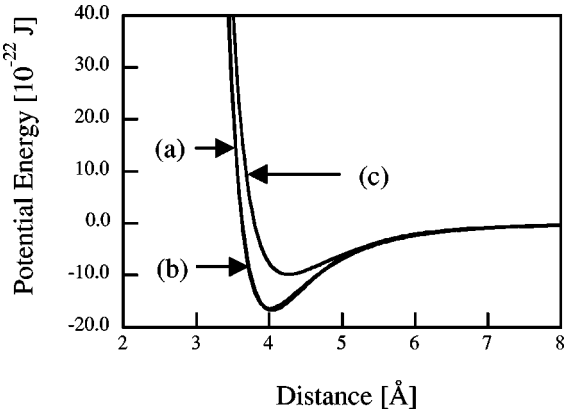

FIG. 2. Potential curves of the averaged AWJ and LJ potential and LJ potential obtained by experiment. (a) averaged AWJ potential; (b) averaged LJ potential with $\sigma_a = 3.17\times10^{-10}$ m and $\varepsilon_a = 6.52\times10^{-22}$ J; (c) LJ potential from the viscosity coefficient with $\sigma_m = 3.80\times10^{-10}$ m and $\varepsilon_m = 9.86\times10^{-22}$ J.

aged LJ potential agree very well with each other even at the potential well. It is also shown that these potentials agree well with the monatomic LJ potential at $R > 5.0$ Å, but they are different from each other near the potential well and the repulsive region. It is important that the intermolecular potential must be described accurately near the potential well for the energy transfer to be calculated accurately. For this reason, the LJ potential obtained by the sum of four interaction potentials from Eq. (1) is used to calculate energy transfer at the collision.

B. Numerical method

The motion of the center of mass of the two collision molecules is described by a coordinate system fixed so that its origin coincides with the center of mass of the system, hereafter called ''space coordinate system.'' The orientation of a rigid body specifies the relation between the space coordinate system and a coordinate system fixed with respect to a molecule so that its origin coincides with the center of mass of the atoms of each molecule and the z-axis coincides with the axis of the molecule, hereafter called ''molecular coordinate system.'' The relationship between the two coordinate systems is described by the Euler angles $(\phi_i, \theta_i, \psi_i)$ of diatomic molecule $i(=1,2)$.[19] The subscript (x,y,z) represents the values in space coordinate system and (x',y',z') in the molecular coordinate system.

The equations of translational motion of molecules 1 or 2 are described in the space coordinate system as

$$m_m \ddot{\boldsymbol{X}}_1 = \sum_{i=1}^{2}\sum_{j=1}^{2} \boldsymbol{F}_{ij}, \quad m_m \ddot{\boldsymbol{X}}_2 = \sum_{i=1}^{2}\sum_{j=1}^{2} (-\boldsymbol{F}_{ij}), \tag{4}$$

where m_m is the mass of a molecule, and $\boldsymbol{X}=(x,y,z)$ is the position of the center of mass of each molecule. $\boldsymbol{F}_{ij}$ is the force which acts between the atom $i(=1,2)$ of molecule 1 and the atom $j(j=1,2)$ of molecule 2. This force is obtained by

$$\boldsymbol{F}_{ij} = -\left.\frac{\partial V}{\partial r}\right|_{r=r_{ij}} \frac{\boldsymbol{r}_{ij}}{r_{ij}} = 24\varepsilon_a \left(2\frac{\sigma_a^{12}}{r_{ij}^{14}} - \frac{\sigma_a^{6}}{r_{ij}^{8}} \right) \boldsymbol{r}_{ij}. \tag{5}$$

The equations of rotational motion of molecules 1 and 2 are described in the molecular coordinate system as

$$\mathcal{I}\dot{\boldsymbol{\omega}}_{1'} = \boldsymbol{T}_{1'}, \quad \mathcal{I}\dot{\boldsymbol{\omega}}_{2'} = \boldsymbol{T}_{2'}, \tag{6}$$

$\mathcal{I}$ denotes the inertia tensor whose components are obtained as $I_{x'x'} = I_{y'y'} = 1/2 m_a r_c^2 (\equiv I)$, $I_{z'z'} = 0$ and $I_{ij}(i \neq j) = 0$ where r_c is the interatomic distance of each molecule and taken to be 1.094 Å for nitrogen,[20] and m_a is the mass of an atom. The torques acting upon molecule 1 are obtained by

$$\begin{aligned} T_{1x'} &= -\frac{r_c}{2}\sum_{j=1}^{2} (F_{1jy'} - F_{2jy'}), \\ T_{1y'} &= \frac{r_c}{2}\sum_{j=1}^{2} (F_{1jx'} - F_{2jx'}), \quad T_{1z'} = 0. \end{aligned} \tag{7}$$

The acting torques for molecule 2 are obtained by replacing subscript 1 in Eqs. (7) with subscript 2 and subscript 2 with subscript 1.

The change of the orientation of molecules and the direction of rotational vector are described as the change of the Euler angle (ϕ, θ, ψ).[19] The parameters ϕ, θ denote the initial orientation of the molecules and ψ denotes the initial direction of rotational vector. In the present study, the quaternion method is used to calculate the change of the Euler angle.[19] The four quaternions $\boldsymbol{q} = (\xi, \eta, \zeta, \chi)$ are defined as

$$\xi_1 = \cos\frac{\theta_1}{2}\cos\frac{\phi_1 - \psi_1}{2}, \tag{8}$$

$$\eta_1 = \sin\frac{\theta_1}{2}\cos\frac{\phi_1 - \psi_1}{2}, \tag{9}$$

$$\zeta_1 = \sin\frac{\theta_1}{2}\sin\frac{\phi_1 + \psi_1}{2}, \tag{10}$$

$$\chi_1 = \cos\frac{\theta_1}{2}\sin\frac{\phi_1 + \psi_1}{2}. \tag{11}$$

The quaternions for each molecule satisfy the equations of motion

$$\begin{pmatrix} \dot{\xi}_1 \\ \dot{\eta}_1 \\ \dot{\zeta}_1 \\ \dot{\chi}_1 \end{pmatrix} = \frac{1}{2}\begin{pmatrix} \xi_1 & -\eta_1 & -\zeta_1 & -\chi_1 \\ \eta_1 & \xi_1 & -\chi_1 & \zeta_1 \\ \zeta_1 & \chi_1 & \xi_1 & -\eta_1 \\ \chi_1 & -\zeta_1 & \eta_1 & \xi_1 \end{pmatrix} \begin{pmatrix} 0 \\ \omega_{1x'} \\ \omega_{1y'} \\ \omega_{1z'} \end{pmatrix}. \tag{12}$$

The quaternions for molecule 2 are also obtained by replacing subscript 1 in Eqs. (8)–(12) with subscript 2.

The diagram of this simulation is shown in Fig. 3. For initial conditions, the relative velocity $\boldsymbol{v}_1$, $\boldsymbol{v}_2(=-\boldsymbol{v}_1)$ is taken to be parallel to the x axis of the space coordinate system. The two molecules are located at a distance of $3\sigma_a$ parallel to the x axis so that the initial interaction potential can be neglected. The initial position vectors of molecule 1 or 2 are given by

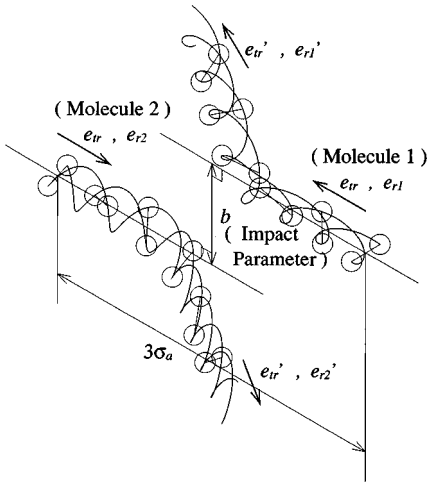

FIG. 3. The collision process of diatomic molecules.

$$x_1=\frac{3}{2}\sigma_a, \quad y_1=\frac{1}{2}b, \quad z_1=0, \tag{13}$$

$$x_2=-\frac{3}{2}\sigma_a, \quad y_2=-\frac{1}{2}b, \quad z_2=0, \tag{14}$$

where b is the initial impact parameter. The initial relative velocity $\boldsymbol{v}_1$, $\boldsymbol{v}_2$ and the initial angular velocity $\boldsymbol{\omega}_1$, $\boldsymbol{\omega}_2$ of molecule 1 or 2, respectively, are given by

$$v_{1x}=-\frac{2e_{\mathrm{tr}}}{m_m}, \quad v_{1y}=0, \quad v_{1z}=0, \tag{15}$$

$$v_{2x}=\frac{2e_{\mathrm{tr}}}{m_m}, \quad v_{2y}=0, \quad v_{2z}=0, \tag{16}$$

$$\omega_{1x'}=\frac{2e_{\mathrm{r1}}}{I}, \quad \omega_{1y'}=0, \quad \omega_{1z'}=0, \tag{17}$$

$$\omega_{2x'}=\frac{2e_{\mathrm{r2}}}{I}, \quad \omega_{2y'}=0, \quad \omega_{2z'}=0, \tag{18}$$

where e_{tr} is the relative translational energy and e_{r1} and e_{r2} are the initial rotational energy of molecule 1 and 2, respectively. In this paper, they are described as the unit of temperature by the following relation:

$$e_{\mathrm{tr}}=\frac{1}{2}kT_{\mathrm{tr}}, \quad e_{\mathrm{r1}}=kT_{\mathrm{r1}}, \quad e_{\mathrm{r2}}=kT_{\mathrm{r2}}. \tag{19}$$

In order to reproduce the realistic collision probability about initial orientation of molecule, the direction of rotational vector and impact parameter the impact parameter b is chosen to be

$$b=b_{\max}\sqrt{R}, \tag{20}$$

and the initial Euler angle of molecule 1 or 2 are chosen to be

$$\phi_1=2\pi R, \quad \theta_1=\cos^{-1}(1-2R), \quad \psi_1=2\pi R, \tag{21}$$

$$\phi_2=2\pi R, \quad \theta_2=\cos^{-1}(1-2R), \quad \psi_2=2\pi R, \tag{22}$$

where $b_{\max}$ is the maximum impact parameter over which the change of state of the collision molecule is negligible and R is a uniform random number in the range of (0,1). In the present study, the set of Eqs. (4) and (6) is numerically solved using the leap-frog method. In this simulation, energy is nondimensionalized by ε_a, length by σ_a, and mass by m_a. The time step $\triangle t$ is chosen $\triangle t=0.1\times10^{-15}$ s for calculation accuracy. The numerical convergence of solutions is confirmed by checking the conservation of total energy. Since the dimensionless total energy changes by less than 10^{-6}, it can be said that the simulation is accurate enough. The MD simulation is completed when the collision molecules are far enough apart from each other to neglect the potential energy between the two molecules. The relative velocity of molecule 1 (v_x',v_y',v_z') and the rotational vector $(\omega_{x'}',\omega_{y'}',\omega_{z'}')$ of molecules 1 and 2 and initial impact parameter b are recorded. The translational and rotational energy after collision is obtained as

$$\begin{aligned} e_{\mathrm{tr}}'&=\tfrac{1}{2}m_m(v_x'^2+v_y'^2+v_z'^2),\\ e_{\mathrm{r1}}'&=\tfrac{1}{2}I(\omega_{1x'}'^2+\omega_{1y'}'^2+\omega_{1z'}'^2),\\ e_{\mathrm{r2}}'&=\tfrac{1}{2}I(\omega_{2x'}'^2+\omega_{2y'}'^2+\omega_{2z'}'^2). \end{aligned} \tag{23}$$

In the present study, the simulations are carried out 10 000 times at one combination of initial energy $(T_{\mathrm{tr}},T_{\mathrm{r1}},T_{\mathrm{r2}})$ by changing the impact parameter according to Eq. (20) and the initial Euler angle from Eqs. (21) and (22). Moreover, the set of simulations must be carried out at various initial energies $(T_{\mathrm{tr}},T_{\mathrm{r1}},T_{\mathrm{r2}})$ to make the data cover the whole range of energy in the DSMC simulation. In the case of 700 K (the maximum temperature at which the vibrational degree of freedom is negligible), the probability for the translational energy T_{tr} to become less than 2000 K is 0.87 and the probability for the rotational energy T_{r1} (or T_{r2}) to become less than 2000 K is 0.94. Therefore, it can be said that the flows at the temperature of middle range can be simulated accurately with the MD data at which the combination of energy is less than 2000 K. Therefore, the set of simulations are carried out at 858 (11×78) combination of initial energy by changing T_{tr} into 50, 100, 150, 200, 400, 600, 800, 1000, 1200, 1600 and 2000 K (11 cases) and T_{r1}, T_{r2} into 0, 50, 100, 150, 200, 400, 600, 800, 1000, 1200, 1600, 2000 K $(12\times11/2+12=78$ cases by identifying the combinations about the exchange between T_{r1} and $T_{\mathrm{r2}})$. In this paper, $b_{\max}$ is given as 3.0 σ_a when T_{tr} is less than 150 K and 2.5 when T_{tr} is more than 200 K. The rotational characteristic temperature of N_2 is 2.878 K and is much lower than 50 K. For this reason, it is valid to consider the rotational energy as a continuous one. The vibrational characteristic temperature of N_2 is 3776 K and is higher than 2000 K. For this reason, it is valid to neglect the vibrational energy.

C. Binary collision of two molecules

Figure 4 shows the time history of the translational, rotational 1 and 2, potential and total energy during the collision of two molecules. The initial energy of the collision molecules is $T_{\mathrm{tr}}=400$ K, $T_{\mathrm{r1}}=400$ K, $T_{\mathrm{r2}}=600$ K in Eq.

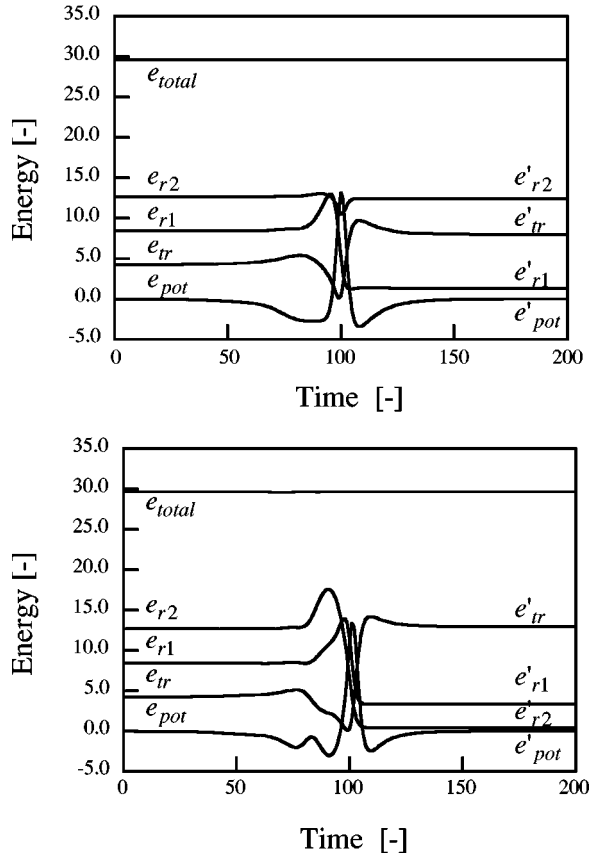

FIG. 4. The typical process of energy transfer at $T_{tr}=400$ K, $T_{r1}=400$ K, $T_{r2}=600$ K, and $b=1.0\sigma_a$. Time is reduced by $\sigma_a\sqrt{m_a/\varepsilon_a}$ and energy by ε_a. In these two figures, the initial orientation of molecules and the initial direction of the rotational vector (the initial Euler angle) are different.

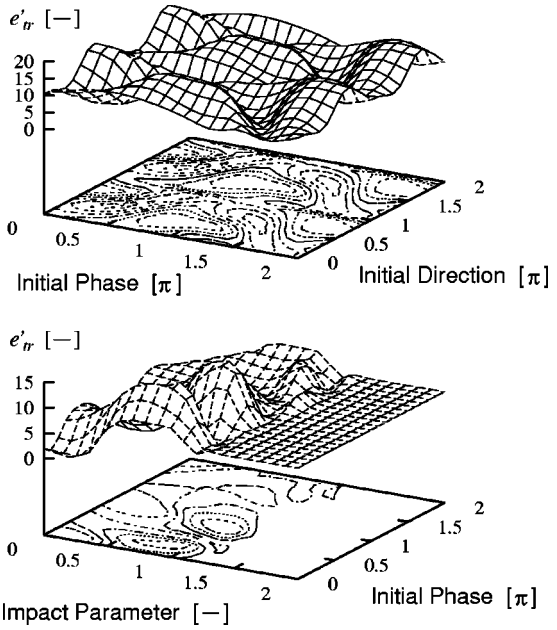

FIG. 5. The effect of initial orientation, initial direction of rotational vector and impact parameter on energy transfer at $T_{tr}=400$ K, $T_{r1}=400$ K and $T_{r2}=600$ K. The translational energy after collision, e'_{tr}, is reduced by ε_a and the impact parameter by σ_a. Upper: translational energy after collision against the initial orientation or initial direction of rotational vector; lower: translational energy after collision against the initial orientation and impact parameter.

(19), and the random number in Eq. (20) is given so that the impact parameter b becomes $1.0\sigma_a$. The initial orientation of molecule and direction of the rotational vector are randomly determined.

As shown in the upper figure, the potential energy e_{pot} decreases and the relative translational energy e_{tr} increases (this means that the molecules fall into the potential well as the molecules approach each other). The molecule passes through the potential well and reaches the repulsive region. The energy transfer between translation and rotation occurs mainly in this region. For this case, the relative translational energy increases and rotational energy of molecules 1 and 2 decrease. The amount of decrease of e_{r1} and e_{r2}, however, is different. At last, the molecule passes through the potential well and the energy of each degree of freedom does not change after the two molecules apart from each other. As shown in the lower figure, the potential energy e_{pot} decreases and the relative translational energy e_{tr} increases like the upper figure. However, the energy after collision in the lower figure is different from that in the upper figure depending upon the initial orientation of the molecules and the direction of the rotational vector, even though the initial translational and rotational energy is the same. It is shown that the total energy is well conserved compared with the amount of energy transfer at the collision. For this reason, the time step Δt is small enough.

In order to study the effect of the initial orientation of the molecule and the direction of the rotational vector, the translational energy after collision is plotted in Fig. 5 for a variety of initial orientations of molecules, initial directions of the rotational vector and the impact parameter. In the upper figure, the random numbers of ϕ_1, ψ_1 in Eq. (21) are varied so that ϕ_1 (which denotes the initial orientation of molecule 1) changes from 0 to 2π and ψ_1 (which denotes the initial direction of rotational vector of molecule 1) changes from 0 to 2π. The impact parameter b is fixed as $1.0\ \sigma_a$. The random number of θ_1 in Eq. (21) and those in Eq. (22) are fixed. In the lower figure, the random numbers of ϕ_1 in Eq. (21) and that of b in Eq. (20) are varied so that ϕ_1 changes from 0 to 2π and b changes from 0 to b_{max}. In this simulation, b_{max} is given as $2.0\ \sigma_a$. The other random number in Eq. (21) and those in Eq. (22) are fixed. In these two figures, the initial energy of the collision molecules is given as $T_{tr}=T_{r1}=T_{r2}=400$ K in Eq. (19).

As shown in the upper figure, the translational energy after collision changes very complicatedly and is sensitive to a small change of the initial orientation of molecules or the initial direction of the rotational vector. The functional relationship is also very complicated. As shown in the lower figure, the translational energy after collision does not change regardless of the initial orientation when the impact parameter is more than about $1.3\ \sigma_a$. The translational energy after collision, however, also changes very complicatedly by changing the initial orientation of the molecule or the impact parameter like the upper figure when the impact parameter is less than about $1.3\ \sigma_a$. Moreover, it is not as important to determine the energy after collision as a func-

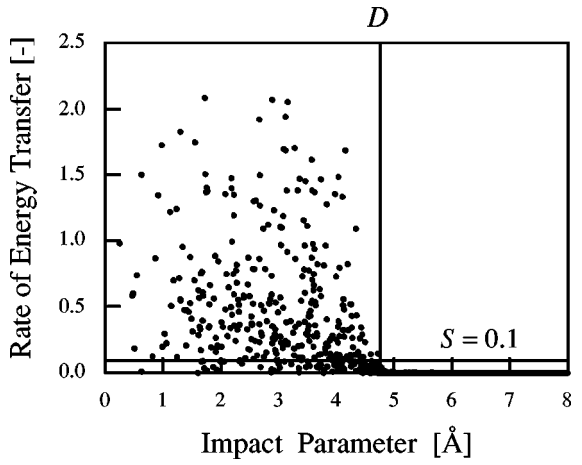

FIG. 6. The rate of translational energy transfer, S, against impact parameter at $T_{tr}=400$ K, $T_{r1}=400$ K and $T_{r2}=600$ K.

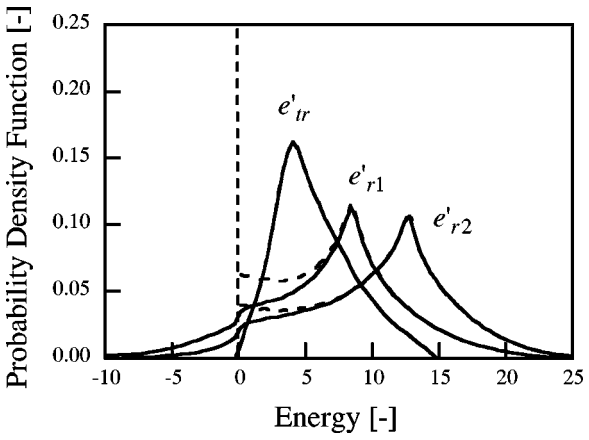

FIG. 7. The probability density functions of translational and rotational energy after collision at $T_{tr}=400$ K, $T_{r1}=400$ K and $T_{r2}=600$ K. Energy is reduced by ε_a and probability density function by $1/\varepsilon_a$. Bold lines: with considering the sign of angular momentum; Dashed lines: without considering the sign of angular momentum.

tion of initial orientation of molecules, the initial direction of the rotational vector or impact parameter except for the flow fields in which the initial orientations, the initial directions of the rotational vector or the impact parameters of the collision molecules are not distributed according to Eqs. (20), (21) and (22) are simulated. Therefore in the DMC model the probability density functions of translational and rotational energy after collision are constructed as a function of only the initial energy (e_{tr},e_{r1},e_{r2}) by integrating the effects of the initial orientation of molecules, the initial direction of the rotational vector and impact parameter.

D. Statistical behavior of the state of molecules after collision

The relation between the impact parameter and the rate of energy transfer is required to estimate the probability density function of energy after collision. Figure 6 shows the rate of translational energy transfer against impact parameter for $T_{tr}=400$ K, $T_{r1}=400$ K, $T_{r2}=600$ K and $b_{max}=3.0\sigma_a$, where the rate of energy transfer is defined as $S=|e'_{tr}-e_{tr}|/e_{tr}$. As shown in this figure, the rate of energy transfer is distributed very widely from 0 to 2.5 when b is less than about 1.5 σ_a. However, the rate of energy transfer converges very rapidly near $b=1.5\sigma_a$ and becomes nearly 0 without deviation when b is more than 1.5 σ_a. These molecules can be considered to not collide with each other. Now define the largest impact parameter at which S is greater than 0.1 as threshold D. The molecules which collide within impact parameter D is defined as ''collision molecules'' and the molecules which collide over D is defined as ''no-collision molecules.''

The probability density functions of translational and rotational energy after collision are defined as the function of only the initial energy (e_{tr},e_{r1},e_{r2}) by the sum of the results of MD simulation of which the impact parameters are less than D. As a result, it is found that the function for the translational and rotational energy distribution has a similar shape in all simulated conditions. A typical result is shown as the dash lines in Fig. 7. As shown in this figure, the probability density functions of translational and rotational energy after collision have their peaks at the initial energy and long tails on both sides. The probability density functions decrease exponentially. In the case of rotational energy, however, the probability near $e=0$ is greater compared with the exponential function. The reason is explained as follows:

Let's consider that the two molecules collide and the rotational energy of molecule 1 changes from $I\omega_{1x'}^2/2$ to $I\omega_{1x'}^2/8$. Two cases are considered in this collision. First, the angular momentum is changed from $(\omega_{1x'},0,0)$ to $(\omega_{1x'}/2,0,0)$ (hereafter called as ''Case 1''). Second, the angular momentum is changed from $(\omega_{1x'},0,0)$ to $(-\omega_{1x'}/2,0,0)$ (hereafter called as ''Case 2''). The two energies after collision are the same in these two cases. The interaction between molecules in Case 2, however, is stronger than that in Case 1. For this reason, the probability of Case 2 becomes smaller than that of Case 1. Therefore, these two cases must be distinguished. In the present paper, the rotational energy after collision is estimated with the sign of the x' component of angular momentum in order to consider the direction of angular momentum. The replotted data of the dash lines of Fig. 7 are shown in the bold lines of this figure. As shown in this figure, the shape of the function is closer to that of the exponential one.

E. Verification of the potential

In order to verify the LJ potential, similar results obtained by the LJ or AWJ potential are compared with each other. The calculation procedure, however, is very complicated and the simulation time is much longer than that for the LJ potential. For this reason, the LJ potential is verified at only a limited number of combinations of initial energy.

The individual collision processes are compared using the LJ and AWJ potentials. The results are shown in Fig. 8. The initial energy is $T_{tr}=400$ K, $T_{r1}=400$ K and $T_{r2}=600$ K. The initial orientation and the direction of rotational vector and impact parameter are the same. As shown

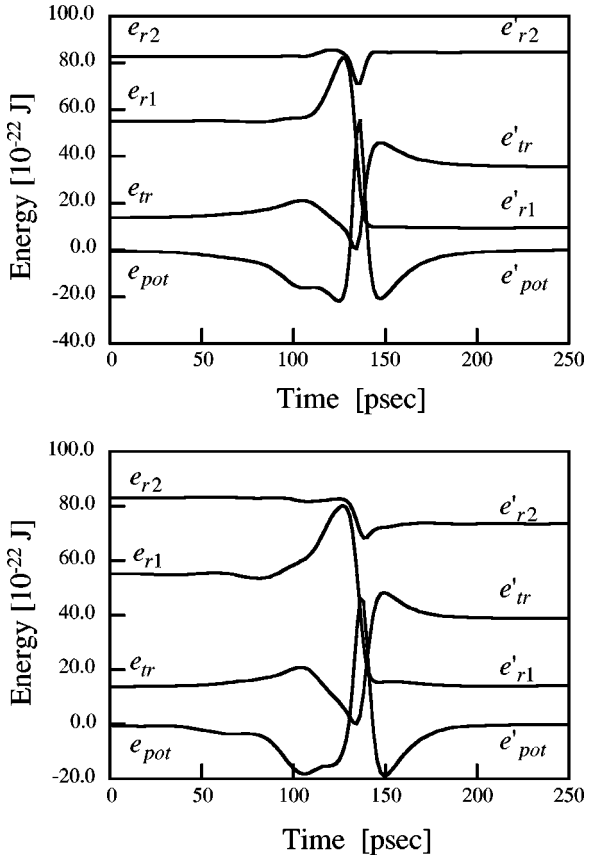

FIG. 8. The energy transfer at collision compared with the LJ and AWJ potential at $T_{tr}=200$ K, $T_{r1}=400$ K and $T_{r2}=600$ K. In these two figures, the random numbers of Eqs. (20)–(22) are the same. Upper: LJ potential; lower: AWJ potential.

in this figure, the energy after collision is different from each other by the difference of potential although the initial conditions are the same.

Then, the probability density functions of translational and rotational energy after collision are compared with each other. Typical results are shown in Fig. 9. The initial energy

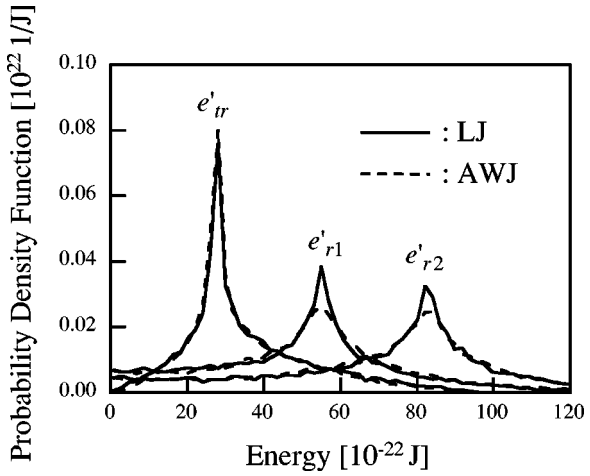

FIG. 9. The probability density functions of translational and rotational energy after collision at $T_{tr}=400$ K, $T_{r1}=400$ K and $T_{r2}=600$ K. compared with the LJ and AWJ potential. In these two figures, the random numbers of Eqs. (20)–(22) are the same.

is $T_{tr}=400$ K, $T_{r1}=400$ K and $T_{r2}=600$ K. The initial orientation of molecule, direction of rotational vector and impact parameter are given as in Eqs. (20)–(22). The number of collision pairs, N, is 128 000. As shown in this figure, the two results agree well with each other. The simulated results at different temperatures show similar results. As shown in these figures, the probability density functions of both the translational and rotational energy after collision agree well with each other even though the individual collision is different. For this reason, the LJ potential function can be used to determine the statistical properties like probability density functions for the energy after collision.

III. DYNAMIC MOLECULAR COLLISION (DMC) MODEL

A. Collision cross sections

In the present paper, the collision cross section is determined based on the equation of the viscosity coefficient of diatomic molecules derived by Wang-Chang and Uhlenbeck.[21,22] The viscosity coefficient μ is obtained by[22]

$$\frac{1}{\mu}=\frac{8}{5\sqrt{2\pi m_a kT}}\int Q_\mu\, d\xi, \tag{24}$$

where k is Boltzmann constant and T is temperature. The integral $\int(\,)d\xi$ specifies

$$\int(\,)d\xi=\frac{2\pi}{S_R^2}\int_0^\infty\int_0^\infty\int_0^\infty(\,)\frac{g^3}{2}J_1J_2 \times\exp\left(-\frac{g^2}{2}-\frac{J_1^2}{2}-\frac{J_2^2}{2}\right)dg\,dJ_1\,dJ_2, \tag{25}$$

where $S_R=4\pi^2IkT$, g is the relative velocity, J_1, J_2 is the angular momenta of molecules 1 and 2, respectively. In Eq. (24), Q_μ is the viscosity cross section, which is the function of relative velocity g and angular momenta J_1, J_2 as

$$Q_\mu=\int\left(\frac{g^4}{4}\sin^2\chi+\frac{1}{3}(\Delta e_r)^2-\frac{1}{2}(\Delta e_r)^2\sin^2\chi\right)d\tau, \tag{26}$$

where $\Delta e_r=e'_{r1}+e'_{r2}-e_{r1}-e_{r2}$ and χ is the scattering angle. The relationship between the rotational energy and angular momentum is obtained as $e_{r1}=J_1^2/2I$ and $e_{r2}=J_2^2/2I$. The integral $\int(\,)d\tau$ mentioned above specifies

$$\int(\,)d\tau=\frac{\pi d^2}{2}\int_0^d\int_{-1}^1\int_{-1}^1\int_0^{2\pi}\int_0^{2\pi}\int_0^{\pi}\int_0^{\pi}(\,) \times\left(\frac{d\phi_1}{\pi}\right)\left(\frac{d\phi_2}{\pi}\right)\left(\frac{d\psi_1}{2\pi}\right)\left(\frac{d\psi_2}{2\pi}\right)\left(\frac{d(\cos\theta_1)}{2}\right) \times\left(\frac{d(\cos\theta_2)}{2}\right)\left(\frac{d(b^2)}{d^2}\right), \tag{27}$$

where ψ represents the initial direction of rotational vector, ϕ and θ represent the initial orientation of molecules, b represents the impact parameter and d is the cutoff impact parameter.

In the previous study,[23,24] the collision cross section is determined so that the viscosity cross section is consistent with that obtained by the realistic intermolecular potential in order to calculate the temperature dependence of the viscosity coefficient accurately. In the present paper, therefore, the collision cross section is determined so that the viscosity cross section of the DMC model is consistent with that obtained by Eq. (26) and the realistic potential defined in Sec. II A. For that purpose, it is necessary to estimate Q_μ in Eq. (26) at a certain combination of translational and rotational energy accurately. In the case of diatomic molecules, however, it is impossible to integrate Eq. (26) analytically because the relationship between the scattering angle χ or the energy after collision $e'_{\rm tr}$, $e'_{\rm r1}$, $e'_{\rm r2}$ and the initial condition is very complicated. For this reason, Q_μ is calculated by the Monte Carlo evaluation of integrals[22] using the MD simulation in Sec. II as

$$Q_{\mu,\mathrm{MD}}=\frac{1}{N}\sum_{i=1}^{N}\left(\frac{g^4}{4}\sin^2\chi_i+\frac{1}{3}(\Delta e_{r,i})^2-\frac{1}{2}(\Delta e_{r,i})^2\sin^2\chi_i\right)d\tau, \tag{28}$$

where N is the number of data. This viscosity cross section $Q_{\mu,\mathrm{MD}}$ converges when $b_{\max}$ is greater so that the effect of potential is neglected.

In the DMC model, the isotropic scattering is assumed like the Variable Hard Sphere (VHS) model[23] for simplicity. In this assumption, $\int \sin^2\chi\ d\tau$ becomes 2/3. For this reason, Eq. (26) becomes

$$Q_{\mu,\mathrm{DSMC}}=\frac{\pi}{12}d^2g^4. \tag{29}$$

The radius of the total collision cross section $d_t(e_{\rm tr},e_{\rm r1},e_{\rm r2})$ is defined as d from Eq. (28) and Eq. (29) so that the viscosity cross section calculated by the DSMC method is consistent with that calculated by the MD method. Therefore,

$$d_t(e_{\rm tr},e_{\rm r1},e_{\rm r2})=\sqrt{\frac{12Q_{\mu,\mathrm{MD}}(e_{\rm tr},e_{\rm r1},e_{\rm r2})}{\pi g^4}}, \tag{30}$$

and the total collision cross section $S_{\rm total}$ is defined by

$$S_{\rm total}=\pi d_t^2. \tag{31}$$

The radius of the total collision cross section against translational energy, $T_{\rm tr}$ is shown in Fig. 10. As shown in this figure, it is found that the total collision cross section decreases as the translational energy increases and it changes depending on not only the translational energy but also rotational energy. The effect of rotational energy is greater as the translational energy decreases.

When the MD data with impact parameters less than d_t are considered to construct the probability density function of energy after collision, it turns out that the shape of the probability density function of energy after collision is similar to the δ-function at low translational energy. It can be easily estimated that a large number of collisions at which the energy is hardly transferred are considered if these MD data are used. If the probability density function is defined using these data, the efficiency of calculation becomes small because many collisions at which the energy is hardly transferred must be calculated in the DSMC simulation. In the present paper, therefore, the inelastic cross section is defined in order to make the simulation time small.

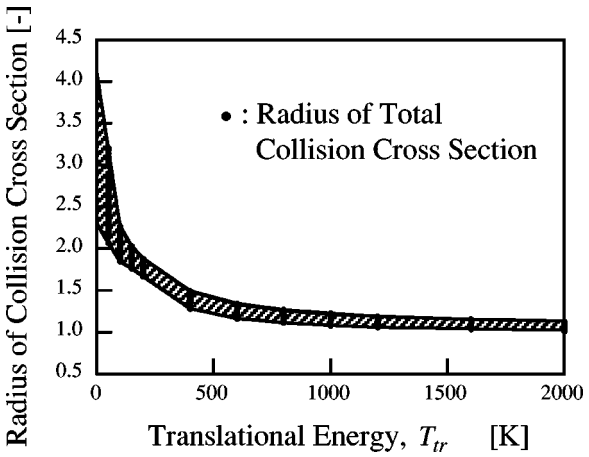

FIG. 10. The radius of total cross section against translational energy. Radius of total collision cross section is reduced by σ_a. The results of 78 combinations of rotational energy are plotted per each translational energy.

Let's consider the value

$$Q_{\rm tr}=\int(\Delta e_{\rm tr})^2 d\tau=\frac{\pi d^2}{2}\frac{1}{N}\sum_{i=1}^{N}(\Delta e_{{\rm tr},i})^2. \tag{32}$$

This value converges as $d\to b_{\max}$. In the present paper, the radius of inelastic cross section d_i is defined as the cutoff impact parameter at which $Q_{\rm tr}$ becomes 95% of the converged value. The inelastic cross section $S_{\rm inel}$ is defined by

$$S_{\rm inel}=\pi d_i^2. \tag{33}$$

The radius of the inelastic collision cross section against translational energy, $T_{\rm tr}$, is shown in Fig. 11. As shown in

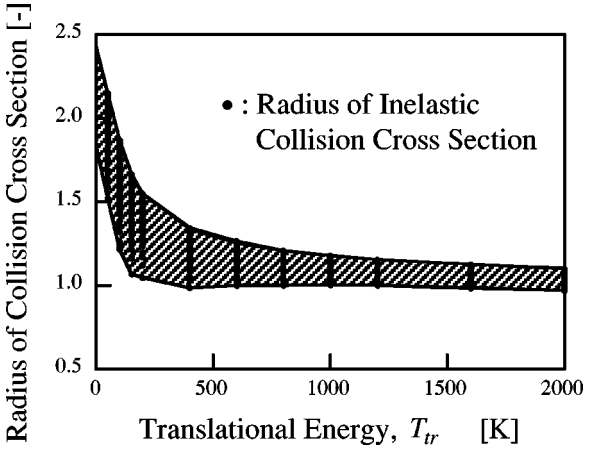

FIG. 11. The radius of inelastic cross section against translational energy. Radius of inelastic collision cross section is reduced by σ_a. The results of 78 combinations of rotational energy are plotted per each translational energy.

this figure, it is found that the difference between the inelastic collision cross section and total cross section increases as the translational energy decreases. It is also found that the inelastic cross section decreases as the translational energy increases and it changes depending on not only the translational energy but also the rotational energy like the total collision cross section. These cross sections, however, change complicatedly as the initial translational energy e_{tr}, and rotational energy e_{r1} or e_{r2} are changed. In the DSMC simulation, it is convenient to calculate and tabulate these parameters beforehand. Consider that the combination of the initial energy, $(e_{\mathrm{tr}},e_{\mathrm{r1}},e_{\mathrm{r2}})$, satisfies the following relation:

$$\begin{aligned} &e_{\mathrm{tr}l}\leqq e_{\mathrm{tr}}<e_{\mathrm{tr}u},\\ &e_{\mathrm{r1}l}\leqq e_{\mathrm{r1}}<e_{\mathrm{r1}u},\\ &e_{\mathrm{r2}l}\leqq e_{\mathrm{r2}}<e_{\mathrm{r2}u}, \end{aligned} \tag{34}$$

where the combinations of energy, $(e_{\mathrm{tr}l},e_{\mathrm{r1}l},e_{\mathrm{r2}l})$ and $(e_{\mathrm{tr}u},e_{\mathrm{r1}u},e_{\mathrm{r2}u})$ are those calculated in Sec. II. The radii of collision cross section, d_t and d_i, are calculated, respectively, as

$$\begin{aligned} d_{t,i}(e_{\mathrm{tr}},e_{\mathrm{r1}},e_{\mathrm{r2}}) &= w_{\mathrm{tr}l}w_{\mathrm{r1}l}w_{\mathrm{r2}l}\,d_{t,i}(e_{\mathrm{tr}l},e_{\mathrm{r1}l},e_{\mathrm{r2}l}) + w_{\mathrm{tr}l}w_{\mathrm{r1}l}w_{\mathrm{r2}u}\,d_{t,i}(e_{\mathrm{tr}l},e_{\mathrm{r1}l},e_{\mathrm{r2}u}) + w_{\mathrm{tr}l}w_{\mathrm{r1}u}w_{\mathrm{r2}l}\,d_{t,i}(e_{\mathrm{tr}l},e_{\mathrm{r1}u},e_{\mathrm{r2}l})\\ &+ w_{\mathrm{tr}l}w_{\mathrm{r1}u}w_{\mathrm{r2}u}\,d_{t,i}(e_{\mathrm{tr}l},e_{\mathrm{r1}u},e_{\mathrm{r2}u}) + w_{\mathrm{tr}u}w_{\mathrm{r1}l}w_{\mathrm{r2}l}\,d_{t,i}(e_{\mathrm{tr}u},e_{\mathrm{r1}l},e_{\mathrm{r2}l}) + w_{\mathrm{tr}u}w_{\mathrm{r1}l}w_{\mathrm{r2}u}\,d_{t,i}(e_{\mathrm{tr}u},e_{\mathrm{r1}l},e_{\mathrm{r2}u})\\ &+ w_{\mathrm{tr}u}w_{\mathrm{r1}u}w_{\mathrm{r2}l}\,d_{t,i}(e_{\mathrm{tr}u},e_{\mathrm{r1}u},e_{\mathrm{r2}l}) + w_{\mathrm{tr}u}w_{\mathrm{r1}u}w_{\mathrm{r2}u}\,d_{t,i}(e_{\mathrm{tr}u},e_{\mathrm{r1}u},e_{\mathrm{r2}u}), \end{aligned} \tag{35}$$

where w's are the ratios obtained by

$$w_{\mathrm{tr}l}=\frac{e_{\mathrm{tr}u}-e_{\mathrm{tr}}}{e_{\mathrm{tr}u}-e_{\mathrm{tr}l}},\quad w_{\mathrm{r1}l}=\frac{e_{\mathrm{r1}u}-e_{\mathrm{r1}}}{e_{\mathrm{r1}u}-e_{\mathrm{r1}l}},\quad w_{\mathrm{r2}l}=\frac{e_{\mathrm{r2}u}-e_{\mathrm{r2}}}{e_{\mathrm{r2}u}-e_{\mathrm{r2}l}}, \tag{36}$$

$$w_{\mathrm{tr}u}=\frac{e_{\mathrm{tr}}-e_{\mathrm{tr}l}}{e_{\mathrm{tr}u}-e_{\mathrm{tr}l}},\quad w_{\mathrm{r1}u}=\frac{e_{\mathrm{r1}}-e_{\mathrm{r1}l}}{e_{\mathrm{r1}u}-e_{\mathrm{r1}l}},\quad w_{\mathrm{r2}u}=\frac{e_{\mathrm{r2}}-e_{\mathrm{r2}l}}{e_{\mathrm{r2}u}-e_{\mathrm{r2}l}}. \tag{37}$$

In the case where the combination of initial energy is out of the table, these values are determined by using these values at $T_{\mathrm{tr}}=T_{\mathrm{r1}}=T_{\mathrm{r2}}=2000\,\mathrm{K}$. Since this collision seldom occurs at the range of temperature, the effect of this procedure is very small.

B. The probability density functions of translational and rotational energy after collision

Considering the data for which impact parameters are less than the radius of inelastic collision cross section, it is found that the probability density functions of translational and rotational energy after collision have similar figures in all simulated conditions as shown in Sec. II D. They have their peaks near the initial energy and they decrease exponentially with a long tail. In the DMC model, the probability density function of energy after collision is constructed by fitting the shape of the MD result using the following exponential function:

$$F(e')=\begin{cases} A_l\exp\{-B_l(e_i-e')\}:\ \text{left side}\\ A_r\exp\{-B_r(e'-e_i)\}:\ \text{right side}, \end{cases} \tag{38}$$

where e_i is the initial translational, rotational 1 or 2 energy and e' is the translational, rotational 1 or 2 energy after collision. The parameters A_l, A_r, B_l and B_r are determined so that the characteristic values of the probability density function obtained by the MD simulation can be calculated by the model function of Eq. (38). In the present paper, the probabilities, P_l and P_r, and the deviations, σ_l and σ_r, are selected as the characteristic values. The probabilities P_l and P_r are calculated by

$$P_l=\frac{N_l}{N_l+N_r},\quad P_r=\frac{N_r}{N_l+N_r}, \tag{39}$$

and the deviations σ_l and σ_r are calculated by

$$\begin{aligned} \sigma_l^2&=\frac{1}{N_l+N_r}\sum_{i=1}^{N_l}(e'-e_i)^2,\\ \sigma_r^2&=\frac{1}{N_l+N_r}\sum_{i=1}^{N_r}(e'-e_i)^2, \end{aligned} \tag{40}$$

where N_l is the number of molecules in which the energy after collision is less than e_i, and N_r is the number of molecules in which the energy after collision is greater than e_i. P_l or P_r is the probability that the energy is less or greater than the initial value, respectively. σ_l^2, σ_r^2 is the deviation of the left and right side of the distribution, respectively. The parameters, A_l, A_r, B_l and B_r are determined so that the following relations are satisfied:

$$\int_a^{e_i}F(e')de'=P_l,\quad \int_{e_i}^{e_{\mathrm{tot}}}F(e')de'=P_r, \tag{41}$$

$$\begin{aligned} &\int_a^{e_i}(e'-e_i)^2F(e')de'=\sigma_l^2,\\ &\int_{e_i}^{e_{\mathrm{tot}}}(e'-e_i)^2F(e')de'=\sigma_r^2. \end{aligned} \tag{42}$$

where a is defined as 0 for the parameters of translational energy and $-e_{\mathrm{tot}}$ for the parameters of rotational 1 or 2 energy. P_l, P_r, σ_l and σ_r of each degree of freedom are calculated at each combination of initial energy $(T_{\mathrm{tr}},T_{\mathrm{r1}},T_{\mathrm{r2}})$. One of these results is shown in Fig. 12. In this figure σ_r^2 of translational energy is plotted by the three dimensional contour at the interval of 2.0 ε_a^2. The three axis

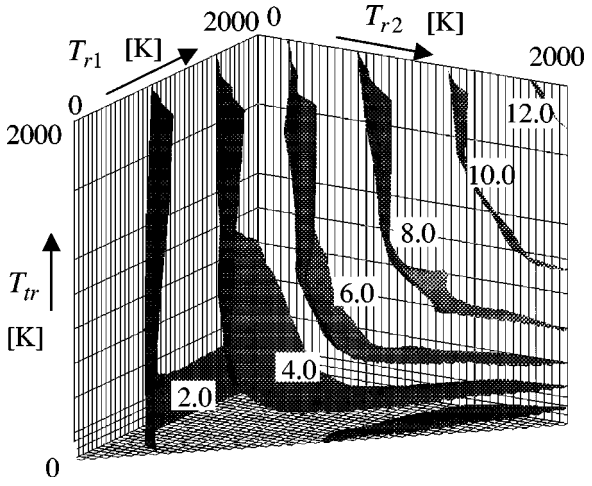

FIG. 12. The three dimensional contour of the right side deviation of probability density function of translational energy, σ_r^2. The tree axis represents the initial translational energy, $e_{\rm tr}$ the rotational 1 and 2 energy, $e_{\rm r1}$ and $e_{\rm r2}$, respectively. Deviation is reduced by ε_a^2. The contours are plotted at $\sigma_r = 2.0$, 4.0, 6.0, 8.0, 10.0 and 12.0.

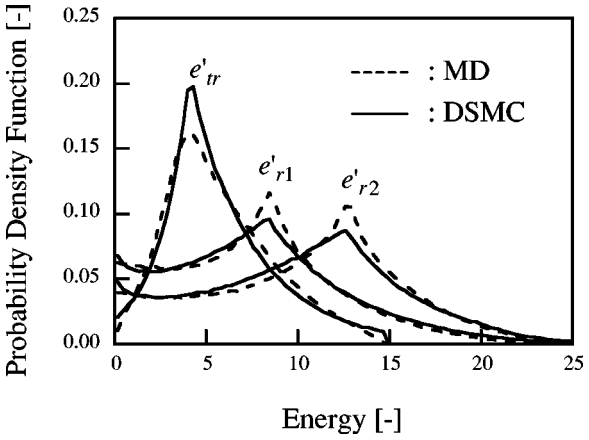

FIG. 13. The energy after collision compared between the DSMC and MD calculation. The combination of initial energy is $T_{\rm tr} = 400$ K, $T_{\rm r1} = 400$ K and $T_{\rm r2} = 600$ K. Energy is reduced by ε_a and probability density function by $1/\varepsilon_a$. Bold lines: DSMC results; Dashed lines: MD results.

represent the initial translational energy $T_{\rm tr}$, rotational 1 energy $T_{\rm r1}$ and 2 $T_{\rm r2}$, respectively. As shown in this figure, σ_r increases as $T_{\rm tr}$ increases at high rotational energy. However, σ_r^2 is less independent of $T_{\rm tr}$ at low rotational energy than at high energy. As shown in this figure, σ_r^2 varies complicatedly as a function of the initial translational and rotational energy and it is impossible to represent this value as the fundamental function of $e_{\rm tr}$, $e_{\rm r1}$ and $e_{\rm r2}$.

In the DSMC simulation, it is also convenient to calculate and tabulate these parameters beforehand like the collision cross sections. The calculation time, however, becomes very large if the parameters P_l, P_r, σ_l and σ_r are used directly because Eqs. (41) and (42) must be calculated by the iterative method. For this reason, $A_{l,r}$ and $B_{l,r}$ at each combination of initial energy are calculated beforehand by Eqs. (38)–(42) and $P'_{l,r}$ and $\sigma'_{l,r}$ are obtained from the following relations:

$$A_{l,r} = \frac{\sqrt{2P'^{\,3}_{l,r}}}{\sigma'_{l,r}}, \quad B_{l,r} = \frac{\sqrt{2P'_{l,r}}}{\sigma'_{l,r}}. \tag{43}$$

These relations correspond to Eqs. (41) and (42) when the integral range is $(-\infty,\infty)$. The values of P'_l, P'_r, σ'_l and σ'_r of the three degrees of freedom (total of 12 parameters at one combination of initial energy) are tabulated and the parameters of model function $A_{l,r}$ and $B_{l,r}$ are calculated by Eq. (43) using linear interpolation like the collision cross sections. In the case where the combination of initial energy is out of the table, these values are determined by using these values at $T_{\rm tr} = T_{\rm r1} = T_{\rm r2} = 2000$ K like the collision cross sections.

To ensure that the total energy is conserved, the total energy $e_{\rm tot}$ is calculated as

$$e_{\rm tot} = 2e_{\rm tr} + e_{\rm r1} + e_{\rm r2} \tag{44}$$

and the energy of each degree of freedom after the collision are redistributed as follows:

• The relative translational energy $e'_{\rm tr}$ is determined using Eq. (38).
• The rest of the energy, $e_{\rm rest}$, is calculated by subtracting $e'_{\rm tr}$ from $e_{\rm tot}$. The rotational 1 energy $e'_{\rm r1}$ is determined from Eq. (38) by substituting $e_{\rm tot}$ in Eqs. (41) and (42) with $e_{\rm rest}$.
• The rotational 2 energy is determined by subtracting $e'_{\rm tr}$ and e'_{r1} from $e_{\rm tot}$.

It is necessary to control the random number R in order to exclude the probabilities that the energy after collision gets a negative value or that the energy after collision is greater than the rest of energy, $e_{\rm rest}$. The probability, S_1, that the energy after collision gets the energy less than a, is obtained by

$$S_1 = \int_{-\infty}^{a} F(e')de' = P'_l \exp\{-B_l(e_i - a)\}, \tag{45}$$

and the probability, S_2, that the energy after the collision is larger than the rest of energy, $e_{\rm rest}$, is obtained by

$$S_2 = \int_{e_{\rm rest}}^{\infty} F(e')de' = \begin{cases} P'_r \exp\{-B_r(e_{\rm rest} - e_i)\} : e_i < e_{\rm rest} \\ P'_l + P'_r - P'_l \exp\{-B_l(e_i - e_{\rm rest})\} : e_i > e_{\rm rest}. \end{cases} \tag{46}$$

In this paper, the random number is controlled as follows so as to avoid these probabilities,

$$R_c = (P'_l + P'_r - S_1 - S_2)R + S_1. \tag{47}$$

Using these equations, the rotational energy after collision takes a negative value because a in Eq. (45) becomes a negative value in the case of rotational energy. In this case the absolute value of this energy is regarded as the rotational energy after collision. Figure 13 shows the probability density function of translational and rotational energy after collision by using this model. The calculation condition is $T_{\rm tr} = 400$ K, $T_{\rm r1} = 400$ K and $T_{\rm r2} = 600$ K. The bold lines repre-

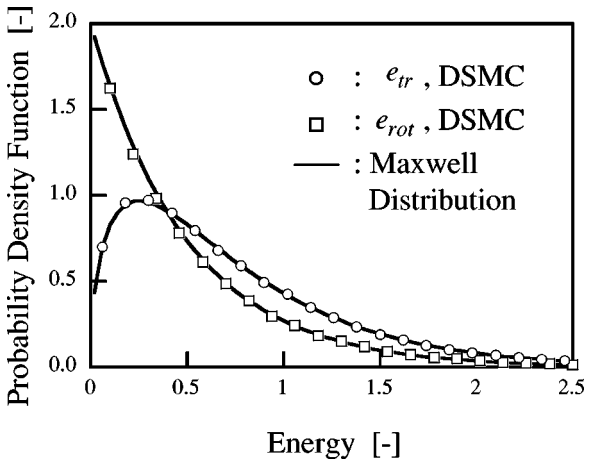

FIG. 14. The energy distribution at equilibrium condition at $T=300$ K. Energy is reduced by $2kT$ and probability density function by $1/2kT$. ○: translational energy distribution by DSMC simulation; □: rotational energy distribution by DSMC simulation; –: Maxwell distribution.

sent the DSMC results and the dash lines represent the MD results. As shown in this figure, the results using this model agree well with the MD data.

IV. VERIFICATION OF THE MODEL

A. The translational and rotational energy distributions at the equilibrium condition

The translational and rotational energy distributions at the equilibrium condition are calculated using the DMC model and the results are compared with theoretical ones. In the DSMC simulation, the null-collision method[17] is used to estimate the collision number. At the equilibrium condition, the translational energy distribution follows the Maxwell distribution as

$$f(e_{\mathrm{tr}})=\frac{2}{kT}\sqrt{\frac{e_{\mathrm{tr}}}{\pi kT}}\exp\left(-\frac{e_{\mathrm{tr}}}{kT}\right), \tag{48}$$

and, since only the rotational degree of freedom is considered and quantum effect is neglected, the rotational energy is distributed by the Maxwell distribution of two degrees of freedom as

$$f(e_{\mathrm{rot}})=\frac{1}{kT}\exp\left(-\frac{e_{\mathrm{rot}}}{kT}\right). \tag{49}$$

As an initial condition, translational energy of each gas molecules is given to $1.5kT$ and rotational energy kT (the initial energy distributions become the δ-function). The simulation is carried out until the energy of the system reaches a steady state. This simulation is carried out in the range of temperature from 300 K to 700 K. The pressure is 1.013×10^5 Pa and the volume is controlled so that the number of molecules, N, becomes 7338. The results are in good agreement with theoretical results. The typical result is shown in Fig. 14. The solid lines denote the theoretical distribution. The open circles represent the translational energy distribution and the open squares represent the rotational energy distribution calculated using the DMC model. As shown in this figure, the simulated values agree well with the theoretical values.

B. Rotational relaxation of nitrogen through normal shock wave

To make sure of the accuracy of this model for nonequilibrium rarefied gas flows, the rotational relaxation of nitrogen through a normal shock wave is examined and the results are compared with experimental results by Robben and Talbot.[10] The coordinate system moves with the wavefront. The x-axis is defined as the direction of the flow. The calculation domain is divided into 201 cells in the x-direction.

Initially, the upstream temperature, T_{in}, upstream pressure, P_{in}, upstream Mach number, M_{in}, are given. The downstream temperature, T_{out}, downstream pressure, P_{out}, flow velocities, u_{in}, u_{out}, number densities, n_{in} and n_{out} and densities ρ_{in} and ρ_{out} are calculated from the equation of state as

$$P_{\mathrm{in}}=n_{\mathrm{in}}kT_{\mathrm{in}}, \quad P_{\mathrm{out}}=n_{\mathrm{out}}kT_{\mathrm{out}}, \tag{50}$$

the definition of Mach number as

$$M_{\mathrm{in}}=\frac{u_{\mathrm{in}}}{c_{\mathrm{in}}}, \quad c_{\mathrm{in}}=\sqrt{\kappa\frac{P_{\mathrm{in}}}{\rho_{\mathrm{in}}}}, \tag{51}$$

and the Rankine–Hugoniot relations as

$$\frac{u_{\mathrm{out}}}{u_{\mathrm{in}}}=\frac{\rho_{\mathrm{in}}}{\rho_{\mathrm{out}}}=1-\frac{2}{\kappa+1}\left(1-\frac{1}{M_{\mathrm{in}}^2}\right), \tag{52}$$

$$\frac{P_{\mathrm{out}}}{P_{\mathrm{in}}}=1+\frac{2\kappa}{\kappa+1}(M_{\mathrm{in}}^2-1), \tag{53}$$

$$\frac{T_{\mathrm{out}}}{T_{\mathrm{in}}}=\left[1+\frac{2\kappa}{\kappa+1}(M_{\mathrm{in}}^2-1)\right]\times\left[1-\frac{2}{\kappa+1}\left(1-\frac{1}{M_{\mathrm{in}}^2}\right)\right], \tag{54}$$

where $\kappa=1.4$ is the ratio of specific heats.

The initial number of molecules in the upstream domain, N_{in}, and the downstream domain, N_{out}, are given as

$$N_{\mathrm{in}}=\mathrm{int}\left(n_{\mathrm{in}}\frac{L}{2}S_a\right), \quad N_{\mathrm{out}}=\mathrm{int}\left(n_{\mathrm{out}}\frac{L}{2}S_a\right), \tag{55}$$

where L denotes the length of the calculation domain and S_a denotes the area. The molecule is randomly distributed at the upstream equilibrium condition in the range of $-L/2<x<0$ and at the downstream equilibrium condition in the range of $0<x<L/2$. The initial velocities in the y- and z-directions are given as the thermal velocities and the initial velocity in the x-direction in the upstream or downstream region is given by adding the thermal velocity and the flow velocity of each domain. The initial rotational energy is distributed by Eq. (49) of each temperature. During the simulation, the number of molecules which enter the upstream boundary, ΔN_{in}, is obtained by

$$\Delta N_{\mathrm{in}}=\frac{n_{\mathrm{in}}S_a\triangle t}{2\beta_{\mathrm{in}}\sqrt{\pi}}K(u_{\mathrm{in}}\beta_{\mathrm{in}}), \tag{56}$$

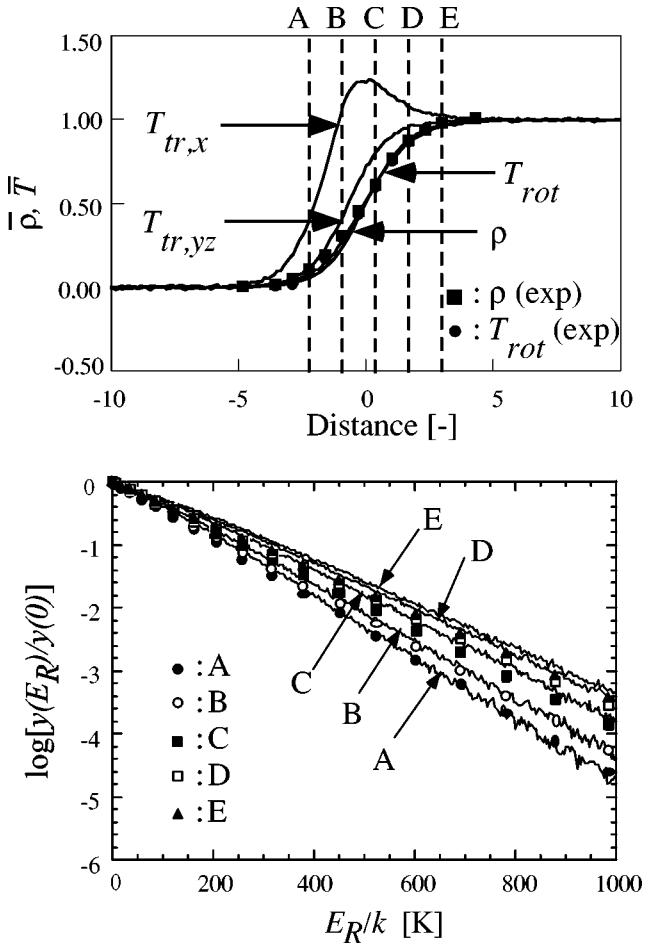

FIG. 15. Shock profiles of one dimensional normal shock wave compared with experimental results. Calculation conditions are $M_{\mathrm{in}}=1.71$, $T_{\mathrm{in}}=202.66$ K, $P_{\mathrm{in}}=7.4030$ Pa, $S_a=3.00\times10^{-16}$ m^2 and $L=20.00\lambda_{\mathrm{in}}$. Upper: number density and temperature profiles; lower: rotational energy distribution in the shock front.

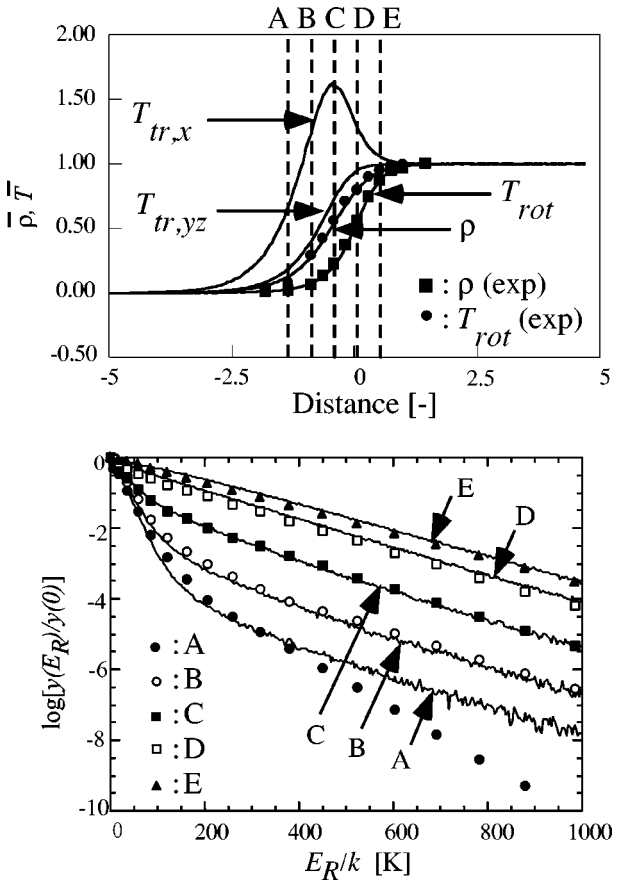

FIG. 16. Shock profiles of one dimensional normal shock wave compared with experimental results. Calculation conditions are $M_{\mathrm{in}}=7.00$, $T_{\mathrm{in}}=28.37$ K, $P_{\mathrm{in}}=0.3704$ Pa, $S_a=3.00\times10^{-16}$ m^2 and $L=10.00\lambda_{\mathrm{in}}$. Upper: number density and temperature profiles; lower: rotational energy distribution in the shock front.

and that which enter the downstream boundary, ΔN_{out}, is obtained by

$$\Delta N_{\mathrm{out}}=\frac{n_{\mathrm{out}}S_a\triangle t}{2\beta_{\mathrm{out}}\sqrt{\pi}}K(-u_{\mathrm{out}}\beta_{\mathrm{out}}), \tag{57}$$

where $K(x)=[\exp(-x^2)-\sqrt{\pi}x\{1+\mathrm{erf}(x)\}]$, $\mathrm{erf}(x)$ is the error function and β_{in} is given as $\beta_{\mathrm{in}}=\sqrt{m/2kT_{\mathrm{in}}}$. The velocity and rotational energy of these molecules are given as the same values as those of the initial conditions. The calculation is carried out until the shock front comes to a stable state, and then a property is sampled. In this paper, the position of the shock front is controlled by making the velocity at the center of the calculation domain equal to $a^*=\sqrt{u_{\mathrm{in}}u_{\mathrm{out}}}$.

The simulations of the rotational relaxation of nitrogen through low and high Mach number shock waves ($M_{\mathrm{in}}=1.71$, 7.00 and 12.9) are performed. The profiles of normalized number density $\overline{n}=(n-n_{\mathrm{in}})/(n_{\mathrm{out}}-n_{\mathrm{in}})$ and translational temperature in the x direction, $\overline{T}_{\mathrm{tr},x}$, that in the y (or z) direction, $\overline{T}_{\mathrm{tr},yz}$ and rotational temperature $\overline{T}_{\mathrm{rot}}$ are shown in the upper figure of Figs. 15–17. The normalized temperature is obtained as $\overline{T}=(T-T_{\mathrm{in}})/(T_{\mathrm{out}}-T_{\mathrm{in}})$ and the temperatures at each cell, $T_{\mathrm{tr},x}$, $T_{\mathrm{tr},yz}$ and T_{rot}, are obtained by the following relations:

$$\frac{1}{2}kT_{\mathrm{tr},x}=\frac{1}{N}\sum\frac{1}{2}m_m(v_x-u_x)^2,\quad kT_{\mathrm{tr},yz}=\frac{1}{N}\sum\frac{1}{2}m_m(v_y^2+v_z^2),\quad kT_{\mathrm{rot}}=\frac{1}{N}\sum e_{\mathrm{rot}}, \tag{58}$$

where N is the number of molecules including in each cell. In these figures, these results are compared with the experimental results of Robben and Talbot,[10] where x is normalized by the upstream mean free path λ_{in}. The calculation conditions are shown in the caption of each figure. The filled squares represent the profile of normalized number density and the filled circles represent the profile of normalized rotational temperature. The calculation results agree well with the experimental results except for the initial rise in the rotational temperature at a low upstream temperature like CTC-DSMC result.[13]

The relaxation of the rotational energy distribution $y(E_R)$ is shown in the lower figure of Figs. 15–17 for Mach 1.71, 7.0 and 12.9 shock waves, respectively, as compared with the experimental data. The symbols in the lower figure

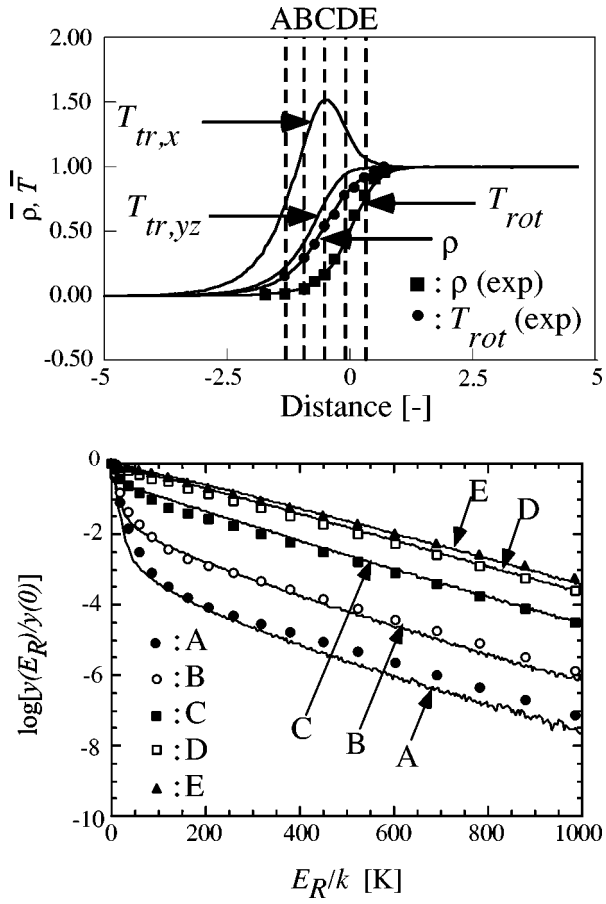

FIG. 17. Shock profiles of one dimensional normal shock wave compared with experimental results. Calculation conditions are $M_{\mathrm{in}}=12.9$, $T_{\mathrm{in}}=8.92$ K, $P_{\mathrm{in}}=0.1014$ Pa, $S_a=3.00\times10^{-16}$ m^2 and $L=10.00\lambda_{\mathrm{in}}$. Upper: number density and temperature profiles; lower: rotational energy distribution in the shock front.

of Figs. 15–17 represents the experimental results of Ref. 10 and the lines represent the calculation results. The energy distributions are plotted at the five points shown in the upper figure, where $y(E_R)$ represents the population of molecules with rotational energy between E_R and $E_R+\Delta E_R$. The statistical errors of the calculation results are very small compared with the results of the CTC-DSMC method[13] because the calculation time of this program is much smaller than the CTC-DSMC method and larger amount of molecules can be sampled. The tendency of the calculation results is very similar to that of the CTC-DSMC method. At a low Mach number, $M_{\mathrm{in}}=1.71$, the plots indicate almost straight lines. At high Mach numbers, $M_{\mathrm{in}}=7.0$, and 12.9, the plots reproduce well the experimentally observed bimodal form. The rotational energy distribution agrees well with the experimental data except at a low upstream temperature in the lower Fig. 16 like the upper figure. The reason is that the equilibrium condition is assumed at the upstream boundary condition although the experimental condition is not an equilibrium condition. These results show that this model can calculate nonequilibrium flows like shock waves very well.

V. CONCLUSION

The inelastic collision of diatomic molecules is simulated using the Molecular Dynamics method and the results are analyzed in detail. The intermolecular potential used in this simulation is the combination of the interatomic Lennard-Jones potential. The potential parameters (σ_a,ε_a) are determined by comparing them with the intermolecular potential based on *ab initio* calculation.

These results show that the amount of energy transferred during the collision is the complicated function of not only the initial translational and rotational energy but also the initial orientation of molecules, the direction of the rotational vector and the impact parameter. However, the probability density function of energy after collision at a certain combination of initial energy has a similar shape. They have their peaks at the initial energy and long tails on both sides. The shape of this function is approximated by an exponential one. The probability density functions are characterized by the initial energy, the probabilites and the deviations.

Using the large amount of data obtained by the MD simulation, the DMC model is constructed. The database of total and inelastic collision cross sections, d_t, d_i, the probabilities, P_l, P_r and deviations σ_l and σ_r are obtained. Those parameters are defined as a function of only the initial translational and rotational energy.

The validity of the DMC model is verified by simulating the translational and rotational energy distributions at the equilibrium condition and the rotational relaxation of nitrogen through normal shock wave. The results are in good agreement with experimental and theoretical results. Consequently, the collision of diatomic molecules can be accurately predicted using the DMC model.

The database of the radius of total collision cross section, d_t, inelastic collision cross section, d_i, the left and right side probabilities of the probability density function of energy after collision, P_l, P_r and the left and right side deviations, σ_l, σ_r can be obtained on an anonymous ftp site at http://medusa.t.u-tokyo.ac.jp/toku/table/.

[1] G. A. Bird, *Molecular Gas Dynamics and the Direct Simulation of Gas Flows* (Clarendon, Oxford, 1994).
[2] K. Nanbu, ''Direct simulation scheme derived from the Boltzmann equation. I. Monocomponent gases,'' J. Phys. Soc. Jpn. **49**, 2042 (1980).
[3] K. Koura, ''A sensitive test for accuracy in evaluation of molecular collision number in the direct simulation Monte Carlo method,'' Phys. Fluids A **2**, 1287 (1990).
[4] P. S. Larsen and C. Borgnakke, ''Statistical collision model for Monte Carlo simulation of polyatomic gas mixture,'' J. Comp. Physiol. **18**, 405 (1975).
[5] J. G. Parker ''Rotational and vibrational relaxation in diatomic gases,'' Phys. Fluids **2**, 449 (1959).
[6] I. D. Boyd, ''Analysis of rotational nonequilibrium in standing shock waves of nitrogen,'' AIAA J. **29**, 1997 (1999).
[7] I. D. Boyd, ''Relaxation of discrete rotational energy distributions using a Monte Carlo method,'' Phys. Fluids A **5**, 2278 (1993).
[8] I. D. Boyd, ''Rotational–translational energy transfer in rarefied nonequilibrium flows,'' Phys. Fluids A **2**, 447 (1990).
[9] I. D. Boyd, ''Temperature dependence of rotational relaxation in shock waves of nitrogen,'' J. Fluid Mech. **246**, 343 (1993).
[10] F. Robben and L. Talbot, ''Experimental study of the rotational distribution function of nitrogen in a shock wave,'' Phys. Fluids **9**, 653 (1966).
[11] K. Koura, ''Statistical inelastic cross-section model for the Monte Carlo simulation of molecules with discrete internal energy,'' Phys. Fluids A **4**, 1782 (1992).
[12] K. Koura, ''Statistical inelastic cross-section model for the Monte Carlo simulation of molecules with continuous internal energy,'' Phys. Fluids A **5**, 778 (1993).

[13]K. Koura, ''Monte Carlo direct simulation of rotational relaxation of diatomic molecules using classical trajectory calculations: Nitrogen shock waves,'' Phys. Fluids **9**, 3543 (1997).
[14]R. M. Berns and A. V. D. Avoird, ''N_2-N_2 interaction potential from *ab initio* calculations, with application to the structure of $(N_2)_2$,'' J. Chem. Phys. **72**, 6107 (1980).
[15]F. Mulder, G. V. Dijk, and A. V. D. Avoird, ''Multipole moments, polarizabilities and anisotropic long range interaction coefficients for N_2,'' Mol. Phys. **39**, 407 (1980).
[16]A. V. D. Avoird, P. E. S. Wormer, and A. P. J. Jansen, ''An improved intermolecular potential for nitrogen,'' J. Chem. Phys. **84**, 1629 (1986).
[17]K. Koura, ''Null-collision technique in the direct-simulation Monte Carlo method,'' Phys. Fluids **29**, 3509 (1986).
[18]R. C. Reid, J. M. Prausnitz, and T. K. Sherwood, *The Properties of Gases and Liquids*, 3rd ed. (McGraw-Hill, New York, 1977).
[19]M. P. Allen and D. J. Tildesley, *Computer Simulation of Liquids* (Clarendon, Oxford, 1987).
[20]G. Herzberg, *Molecular Spectra and Molecular Structure, I. Spectra of Diatomic Molecules*, 2nd ed. (Krieger, Malabar, FL, 1989).
[21]C. S. Wang and G. E. Uhlenbeck, ''Transport phenomena in polyatomic gases,'' Michigan University Engineering Research Institute Report No. CM-681 (1951).
[22]J. A. Lordi and R. E. Mates, ''Rotational relaxation in nonpolar diatomic gases,'' Phys. Fluids **13**, 291 (1970).
[23]G. A. Bird, ''Monte Carlo simulation in an engineering context,'' Prog. Astronaut. Aeronaut. **74**, 239 (1981).
[24]K. Koura and H. Matsumoto, ''Variable soft sphere molecular model for inverse-power-law or Lennard-Jones potential,'' Phys. Fluids A **3**, 2459 (1991).